Determination of crystallographic chirality of MnSi thin film grown on Si (111) substrate

Daisuke Morikawa, Yuichi Yamasaki, Naoya Kanazawa, Tomoyuki Yokouchi, Yoshinori Tokura, and Taka-hisa Arima

Phys. Rev. Materials **4**, 014407 — Published 21 January 2020

DOI: 10.1103/PhysRevMaterials.4.014407

Determination of crystallographic chirality of MnSi thin film grown on Si (111) substrate

Daisuke Morikawa[1†], Yuichi Yamasaki[1,2,3], Naoya Kanazawa[2], Tomoyuki Yokouchi[2], Yoshinori Tokura[1,2], and Taka-hisa Arima[1,4]

[1]*RIKEN Center for Emergent Matter Science (CEMS), Wako 351-0198, Japan*

[2] *Department of Applied Physics and Quantum Phase Electronics Center (QPEC), University of Tokyo, Tokyo 113-8656, Japan*

[3] *Research and Services Division of Materials Data and Integrated System (MaDIS), National Institute for Materials Science (NIMS), Tsukuba 305-0047, Japan*

[4] *Department of Advanced Materials Science, University of Tokyo, Kashiwa 277-8561, Japan*

Abstract

MnSi is a prototypical chiral cubic magnet, in which swirling magnetic objects referred to as magnetic skyrmions appear. It is expected that the thin film of MnSi may expand the range of magnetic skyrmion lattice phase in the temperature-magnetic-field diagram. On the other hand, the MnSi film on an achiral Si (111) substrate may suffer from chiral twin formation. We succeeded in visualizing the domain structure about the chirality and axis-orientation of a MnSi thin film by using the combination of transmission electron microscopy and X-ray reflectivity (XRR) measurement. Only two types of domains were found on a Si (111) substrate. The information is essential for the challenge toward the homochiral film fabrication.

KEYWORDS: Crystallographic chirality, Electron diffraction, Magnetic skyrmion

Present Addresses

†Institute of Multidisciplinary Research for Advanced Materials, Tohoku University, 2-1-1 Katahira, Aoba-ku, Sendai 980-8577, Japan.

Magnetic skyrmions have been extensively studied due to possible applications for new data storage [1-4]. They are observed in chiral magnetic materials with Dzyaloshinskii-Moriya interaction [5-11], dipolar magnets [12-14], interfaces between a paramagnetic metallic layer and a ferromagnetic layer [15-19], and so on. Cubic magnets with a chiral structure are known to host magnetic skyrmions in a magnetic field. However, the thermally equilibrium magnetic skyrmion lattice appears only in a narrow temperature range just below the magnetic transition temperature. In thin films, in contrast, the temperature ranges are observed to expand [20-24].

There are several reports on the growth of thin films of B20-type chiral intermetallic compounds such as FeGe and MnSi on achiral Si (111) substrates [25-32]. Although Si crystal has a large advantage of low defect concentration, the achiral structure may introduce enantiomorphic twins in the thin film. Because a magnetic skyrmion cannot move across the chiral domain boundary, the characterization of chiral twin structure in the film is important for exploring skyrmion functions. Although the atomic displacements and arrangements near the interface were studied by using x-ray and scanning tunneling microscopy (STM) [33], the possible domain structure was not discussed.

In the case of a bulk single crystal, the determination of spin chirality is enough for the determination of crystal chirality, especially for B20-type chiral compounds, because of one-to-one correspondence between crystal chirality and spin chirality [34-37]. However, in the case of chiral twin state, spin helicity determination using a probe with a spatial resolution worse than the typical size of domains such as neutron scattering cannot determine the chirality for each single domain. A useful method to determine the crystal chirality in the thin-film form with a nano meter resolution is electron diffraction. A chirality determination and a chiral-domain analysis were performed by using transmission electron microscopy (TEM) [25] and/or electron back scatter diffraction (EBSD) [38] so far. In principle, EBSD can also identify the crystal-chirality domain by a comparison with simulation using dynamical scattering theory. The difference in EBSD between crystal chirality twins should only appear in the Kikuchi patterns [39]. In the case of TEM observation, a quantitative comparison is needed to determine the chiral structure. However, no evidence was provided in the report that the observed dark-field TEM images should be attributed to the enantiomorphic twins. Karfu et al. first reported the chiral domain structure in a MnSi thin film [25]. However, this report included an error for indexing and a misunderstanding for the origin of contrast in dark-field TEM images. In principle the positions of diffraction spots are not related with the

crystal chirality. The information on the chirality is only included in the intensities of the spots. Convergent-beam electron diffraction (CBED) is another tool for investigating the chirality. Nonetheless, it is difficult to distinguish the handedness of a MnSi thin film grown on a substrate with [111] incidence [40, 41] because the intensity of the electron diffraction from the thin film is strongly affected by the substrate. The specimen must be thicker than several tens nanometer to detect a significant difference between the two enantiomers [42]. It should also be noted that the crystal-axis orientation could be rotated by 60 degrees. In fact, a previous study reported the chiral domain structure with rotated crystal axes [43]. Table 1 compares some methodologies to determine the crystal chirality, domain structure, and interface in plane-view of a thin-film on a substrate. Each of them has advantages and disadvantages. Some limitations are explained at the capture. In this paper, we discuss how to analyze the crystal orientation and chirality in a B20-type MnSi thin film grown on a Si (111) substrate. We investigate whether the diffraction pattern taken with one crystal chirality can be reproduced by using different crystal chirality with the other crystal orientation [40].

A MnSi thin film with 10-nm thickness was grown on a Si (111)-(7×7) substrate by solid phase epitaxy [30]. We first deposited 4-monolayer (ML) Mn atoms at room temperature on the Si substrate followed by annealing for 4 minutes at 200℃ to form a seed layer. Then, 5-ML Mn and 5-ML Si atoms were alternately deposited at room temperature until the prescribed thickness was reached, which was followed by an annealing procedure for 5 minutes at 300℃. The crystal axes of the MnSi thin film show a +30° or −30° rotation around the [111] axis from those of the Si substrate and the in-plane tensile strain was introduced from the difference of lattice parameters between Si = 5.431 Å and MnSi = 4.703 Å. The TEM specimen was prepared by mechanical polishing and Ar ion sputtering with an acceleration voltage of 4 kV. All processes were applied only to the substrate side. Due to the lattice mismatch between Si substrate and MnSi, the area thinner than around 50 nm was heavily bending. We hence performed TEM experiments on a thicker part than 100 nm to avoid the bending effect. Electron diffraction patterns and TEM images were obtained using a TEM (JEOL JEM-2100F) at an acceleration voltage of 200 kV. For the simulation of electron diffraction patterns, we used a software MBFIT developed by Tsuda and Tanaka [44] based on the Bethe matrix method. Synchrotron X-ray experiments were performed at BL-3A, Photon Factory, KEK, Japan, on the same batch of thin film as the TEM experiment. In this paper, we defined the MnSi structure of $P2_13$ with $x_{Mn} = 0.138$ and $x_{Si} = 0.846$ as right-handed and the one with $x_{Mn} = 0.862$ and $x_{Si} = 0.154$ as left-handed, respectively [45].

Figure 1(a) shows a selected area electron diffraction (SAED) pattern at room temperature with the [111] incidence. Indices labeled with Si are based on the Si substrate while others on the MnSi film. Reflections surrounded by yellow circles correspond to positions where reflections from Si substrate and MnSi thin film are expected to be overlapped with each other. Black circles indicate reflections of MnSi thin film, where Si fcc lattice does not satisfy the reflection condition. The diffraction pattern has no mirror symmetry with respect to the vertical $[\,01\bar{1}\,]_{Si}$ axis. Therefore, the clockwise and counter-clockwise rotations around the vertical axis are not equivalent with each other. Figure 1(b) shows an electron diffraction pattern tilted by about 22° around the vertical axis. This diffraction pattern can be considered as the superposition of two diffraction patterns shown in Fig. 1(c). Under this condition, the Si substrate does not show any reflections except for $02\bar{2}$ and $0\bar{2}2$. Reflections surrounded by red (A) and blue (B) circles originate from MnSi with different orientations of crystal axes. Figure 1 (d) shows a convergent-beam electron diffraction pattern with the [111] incidence at room temperature. The observed profile is mainly attributed to the Si substrate because the MnSi thin film is only 10 nm thick in the total thickness of more than 150 nm. Figure 1 (e) shows a simulated CBED pattern of Si. Black and gray arrow heads are eye-guides to distinguish the crystal axis. From the intensity distribution, the crystal axis of Si substrate can be uniquely determined.

Figure 2 summarizes possible crystal configurations for each crystal chirality. It should be noted here that the chiral cubic system with the space group of $P2_13$ has no four-fold axis. As a consequence, $[111]_{Si}$ incidences have two kinds of non-equivalent sets; $\{[111], [\bar{1}\bar{1}1], [\bar{1}1\bar{1}], [1\bar{1}\bar{1}]\}$ and $\{[\bar{1}11], [1\bar{1}1], [11\bar{1}], [\bar{1}\bar{1}\bar{1}]\}$, which is discussed in detail in terms of Bijvoet pair [36]. In the electron diffraction pattern shown in Fig. 1(a), the crystal principal axes of MnSi are rotated by +30° or −30° with respect to the Si substrate. Thus, there are four possible cases with different crystal configurations and zone axis for each crystal chirality. Simulated electron diffraction patterns with a thickness of 10 nm for the zone axis ([111] or $[\bar{1}\bar{1}\bar{1}]$ incidence) and the condition of 22° tilt are listed in Fig. 2. The tilt condition is the same as that in Fig. 1(b). The incidence direction after the tilting depends on the initial zone axis. For example, the [111] incidence is changed to the [312] incidence after the tilting if the MnSi crystal axes are rotated by +30° around the Si [111] axis. The diffraction patterns with the zone axis show a three-fold intensity distribution, which are marked as dotted triangles, while the reflection positions are six-fold. This feature is observed only if the sample is thinner than about 15 nm. It was impossible to determine uniquely the

chirality and the beam incidence direction based only on the zone-axis-incidence pattern, because reflections of a thin film were very weak, and their intensities were dependent on both of crystal-axis orientation and crystal chirality. The diffraction patterns under the tilted condition provide some information about the orientation of the crystallographic axis, which are highlighted by parallelograms. It is noteworthy here that domains rotated by 60 degrees show different intensity distribution both at [111] (or [-1-1-1]) incidence and at the tilted condition if the chirality is the same. When the domains have different chirality, the intensity distribution for the 60-degree rotated structure shows a similar tendency, and this situation is exactly what we observed experimentally. The comparison between the observed diffraction patterns and the simulated patterns for the zone-axis incidence and the tilted incidence clearly excludes two among four configurations for each crystallographic chirality. The crystallographic configurations which agree with the electron diffraction experiments are surrounded by red and blue rounded rectangles in Fig. 2. Hereafter, they are denoted as A1, A2, B1, and B2, respectively. Here it is of note that both the diffraction patterns of the zone-axis incidence and the tilted incidence are necessary to determine the relative orientations of the substrate and the thin film.

Figures 3 (a) and (b) show dark-field TEM images obtained using reflections A and B in Fig. 1 (b), respectively. These images show opposite contrast to each other and correspond to the chiral domains. In this sample, submicron-scale chiral domains are observed at all the specimen without any clear preferred orientation of the domain wall. The area of mono chiral domains is large enough to host magnetic skyrmion lattice. In a small area, the contrast is not reversed. The cause is probably a thin film defect or misorientation of thin film.

To determine the domain set uniquely, we performed an x-ray reflectivity (XRR) measurement. The interference between scattering from MnSi thin film and truncation rod scattering from Si substrate includes the information about stacking manner of MnSi near the interface. Note that the structural factor for x-ray reflectivity depends on the atomic coordinates normal to the surface, but not on the in-plane structure [46,47]. Figure 4 shows the obtained profile of x-ray reflectivity compared with the calculated reflective profiles for the structural models of A1 (B1) and A2 (B2). The influence of the interference scattering is manifested in scattering intensity of the Laue oscillations around MnSi (111). As shown in Fig. 4 (b), the configuration A2 (B2) reproduces better the experimental result than A1 (B1) does.

Figure 5 schematically shows the crystal and chiral structures for A1, A2, B1, and B2 with assuming of an interface structure. Yellow spheres are Si atoms of the substrate. The

atomic arrangement normal to the surface is different between A1 (B1) and A2 (B2). The distance between the bottom Si atoms of MnSi and the top Si atoms with a dangling bond of the substrate for A1 (B1) configuration is different from that for A2 (B2). In this schematic model, the distance is about 2.6 Å and 1.8 Å, respectively. It is expected that A2 and B2 should have exactly the same energy because they are superimposed on each other by a mirror operation. One of such mirror planes is the $(01\bar{1})$ plane of Si substrate, which corresponds to the vertical flip in Fig. 5. In other words, the configurations of A2 and B2 can be regarded as a chiral twin pair.

In conclusion, we visualize the enantiomorphic twin domain structure of a MnSi thin film grown on a (111) Si substrate. By using SAED and x-ray reflectivity measurements we conclude that the observed domain structure should be attributed to chirality twins. Only two kinds of crystallographic domains are present, which are the mirror images of each other.

Acknowledgment

The authors would like to thank Materials Characterization Support Unit, RIKEN for careful maintenance of TEM, and T. Nakajima, K. Tsuda for fruitful discussions. The images of crystal structures were drawn using the software VESTA [48]. Synchrotron X-ray measurement were performed at Photon Factory, KEK (Project No. 2015S2-007). This study was supported by the JSPS Grant-in-Aid for Scientific Research (No. 16H05990, 18K13497) and JST CREST Grant Number JPMJCR1874, Japan.

References

[1] T. H. R. Skyrme, Nucl. Phys. **31**, 556 (1962).

[2] A. N. Bogdanov and D. A. Yablonskii, Zh. Eksp. Teor. Fiz **68**, 101 (1989).

[3] U. K. Rößler, A. N. Bogdanov, and C. Pfleiderer, Nature **442**, 797 (2006).

[4] N. Nagaosa and Y. Tokura, Nat. Nanotechnol. **8**, 899 (2013).

[5] S. Muhlbauer, B. Binz, F. Jonietz, C. Pfleiderer, A. Rosch, A. Neubauer, R. Georgii, and P. Boni, Science (80-.). **323**, 915 (2009).

[6] C. Pfleiderer, T. Adams, A. Bauer, W. Biberacher, B. Binz, F. Birkelbach, P. Böni, C. Franz, R. Georgii, M. Janoschek, F. Jonietz, T. Keller, R. Ritz, S. Mühlbauer, W. Münzer, A. Neubauer, B. Pedersen, and A. Rosch, J. Phys. Condens. Matter **22**, 164207 (2010).

[7] X. Z. Yu, Y. Onose, N. Kanazawa, J. H. Park, J. H. Han, Y. Matsui, N. Nagaosa, and Y. Tokura, Nature **465**, 901 (2010).

[8] S. Seki, X. Z. Yu, S. Ishiwata, and Y. Tokura, Science (80-.). **336**, 198 (2012).

[9] N. Kanazawa, J.-H. Kim, D. S. Inosov, J. S. White, N. Egetenmeyer, J. L. Gavilano, S. Ishiwata, Y. Onose, T. Arima, B. Keimer, and Y. Tokura, Phys. Rev. B **86**, 134425 (2012).

[10] Y. Tokunaga, X. Z. Yu, J. S. White, H. M. Rønnow, D. Morikawa, Y. Taguchi, and Y. Tokura, Nat. Commun. **6**, 7638 (2015).

[11] I. Kézsmárki, S. Bordács, P. Milde, E. Neuber, L. M. Eng, J. S. White, H. M. Rønnow, C. D. Dewhurst, M. Mochizuki, K. Yanai, H. Nakamura, D. Ehlers, V. Tsurkan, and A. Loidl, Nat. Mater. **14**, 1116 (2015).

[12] X. Yu, M. Mostovoy, Y. Tokunaga, W. Zhang, K. Kimoto, Y. Matsui, Y. Kaneko, N. Nagaosa, and Y. Tokura, Proc. Natl. Acad. Sci. **109**, 8856 (2012).

[13] M. Nagao, Y. So, H. Yoshida, M. Isobe, T. Hara, K. Ishizuka, and K. Kimoto, Nat. Nanotechnol. **8**, 325 (2013).

[14] M. Finazzi, M. Savoini, A. R. Khorsand, A. Tsukamoto, A. Itoh, L. Duò, A. Kirilyuk, T. Rasing, and M. Ezawa, Phys. Rev. Lett. **110**, 177205 (2013).

[15] S. Heinze, K. von Bergmann, M. Menzel, J. Brede, A. Kubetzka, R. Wiesendanger, G. Bihlmayer, and S. Blügel, Nat. Phys. **7**, 713 (2011).

[16] N. Romming, C. Hanneken, M. Menzel, J. E. Bickel, B. Wolter, K. von Bergmann, A. Kubetzka, and R. Wiesendanger, Science (80-.). **341**, 636 (2013).

[17] J. Sampaio, V. Cros, S. Rohart, A. Thiaville, and A. Fert, Nat. Nanotechnol. **8**, 839 (2013).

[18] W. Jiang, P. Upadhyaya, W. Zhang, G. Yu, M. B. Jungfleisch, F. Y. Fradin, J. E. Pearson, Y. Tserkovnyak, K. L. Wang, O. Heinonen, S. G. E. Velthuis, A. Hoffmann, S. G. E. te Velthuis, and A. Hoffmann, Science (80-.). **349**, 283 (2015).

[19] S. Woo, K. Litzius, B. Krüger, M. Im, L. Caretta, K. Richter, M. Mann, A. Krone, R. M. Reeve, M. Weigand, P. Agrawal, I. Lemesh, M. Mawass, P. Fischer, M. Kläui, and G. S. D. Beach, Nat. Mater. **15**, 501 (2016).

[20] S. X. Huang and C. L. Chien, Phys. Rev. Lett. **108**, 267201 (2012).

[21] M. N. Wilson, E. A. Karhu, A. S. Quigley, U. K. Rößler, A. B. Butenko, A. N. Bogdanov, M. D. Robertson, and T. L. Monchesky, Phys. Rev. B **86**, 144420 (2012).

[22] Y. Li, N. Kanazawa, X. Z. Yu, A. Tsukazaki, M. Kawasaki, M. Ichikawa, X. F. Jin, F. Kagawa, and Y. Tokura, Phys. Rev. Lett. **110**, 117202 (2013).

[23] S. L. Zhang, I. Stasinopoulos, T. Lancaster, F. Xiao, A. Bauer, F. Rucker, A. A. Baker, A. I. Figueroa, Z. Salman, F. L. Pratt, S. J. Blundell, T. Prokscha, A. Suter, J. Waizner, M. Garst, D. Grundler, G. Van Der Laan, C. Pfleiderer, and T. Hesjedal, Sci. Rep. **7**, 123 (2017).

[24] J. C. Gallagher, K. Y. Meng, J. T. Brangham, H. L. Wang, B. D. Esser, D. W. McComb, and F. Y. Yang, Phys. Rev. Lett. **118**, 027201 (2017).

[25] E. Karhu, S. Kahwaji, T. L. Monchesky, C. Parsons, M. D. Robertson, and C. Maunders, Phys. Rev. B **82**, 184417 (2010).

[26] E. A. Karhu, S. Kahwaji, M. D. Robertson, H. Fritzsche, B. J. Kirby, C. F. Majkrzak, and T. L. Monchesky, Phys. Rev. B **84**, 060404(R) (2011).

[27] E. A. Karhu, U. K. Rößler, A. N. Bogdanov, S. Kahwaji, B. J. Kirby, H. Fritzsche, M. D. Robertson, C. F. Majkrzak, and T. L. Monchesky, Phys. Rev. B **85**, 094429 (2012).

[28] N. A. Porter, G. L. Creeth, and C. H. Marrows, Phys. Rev. B **86**, 064423 (2012).

[29] M. N. Wilson, E. A. Karhu, D. P. Lake, A. S. Quigley, S. Meynell, A. N. Bogdanov, H. Fritzsche, U. K. Rößler, and T. L. Monchesky, Phys. Rev. B **88**, 214420 (2013).

[30] T. Yokouchi, N. Kanazawa, A. Tsukazaki, Y. Kozuka, M. Kawasaki, M. Ichikawa, F. Kagawa, and Y. Tokura, Phys. Rev. B **89**, 064416 (2014).

[31] T. Yokouchi, N. Kanazawa, A. Tsukazaki, Y. Kozuka, A. Kikkawa, Y. Taguchi, M. Kawasaki, M. Ichikawa, F. Kagawa, and Y. Tokura, J. Phys. Soc. Japan **84**, 104708 (2015).

[32] N. Kanazawa, J. S. White, H. M. Rønnow, C. D. Dewhurst, Y. Fujishiro, A. Tsukazaki, Y. Kozuka, M. Kawasaki, M. Ichikawa, F. Kagawa, and Y. Tokura, Phys. Rev. B **94**, 184432 (2016).

[33] B. Geisler, P. Kratzer, T. Suzuki, T. Lutz, G. Costantini, and K. Kern, Phys. Rev. B **86**, 115428 (2012).

[34] M. Tanaka, H. Takayoshi, M. Ishida, and Y. Endoh, J. Phys. Soc. Japan 54, 2970 (1985).

[35] M. Ishida, Y. Endoh, S. Mitsuda, Y. Ishikawa, and M. Tanaka, J. Phys. Soc. Japan 54, 2975 (1985).

[36] S. V Grigoriev, D. Chernyshov, V. A. Dyadkin, V. Dmitriev, S. V Maleyev, E. V Moskvin, D. Menzel, J. Schoenes, and H. Eckerlebe, Phys. Rev. Lett. 102, 037204 (2009).

[37] S. V Grigoriev, D. Chernyshov, V. A. Dyadkin, V. Dmitriev, E. V Moskvin, D. Lamago, T. Wolf, D. Menzel, J. Schoenes, S. V Maleyev, and H. Eckerlebe, Phys. Rev. B 81, 012408 (2010).

[38] A. I. Figueroa, S. L. Zhang, A. A. Baker, R. Chalasani, A. Kohn, S. C. Speller, D. Gianolio, C. Pfleiderer, G. van der Laan, and T. Hesjedal, Phys. Rev. B **94**, 174107 (2016).

[39] A. Winkelmann and G. Nolze, Ultramicroscopy **149**, 58 (2015).

[40] H. Inui, A. Fujii, K. Tanaka, H. Sakamoto, and K. Ishizuka, Acta Crystallogr. Sect. B Struct. Sci. **59**, 802 (2003).

[41] A. W. S. Johnson, Acta Crystallogr. Sect. B Struct. Sci. **63**, 511 (2007).

[42] D. Morikawa, K. Shibata, N. Kanazawa, X. Z. Yu, and Y. Tokura, Phys. Rev. B **88**, 024408 (2013).

[43] M. Trabel, N. V Tarakina, C. Pohl, J. A. Constantino, C. Gould, K. Brunner, and L. W. Molenkamp, J. Appl. Phys. **121**, 245310 (2017).

[44] K. Tsuda and M. Tanaka, Acta Crystallogr. Sect. A Found. Crystallogr. **55**, 939 (1999).

[45] M. Tanaka, H. Takayoshi, M. Ishida, and Y. Endoh, J. Phys. Soc. Japan **54**, 2970 (1985).

[46] Y. Yacoby, M. Sowwan, E. Stern, J. O. Cross, D. Brewe, R. Pindak, J. Pitney, E. M. Dueresne, and R. Clarke, Nat. Mater. 1, 99 (2002).

[47] H. Morisaki, T. Koretsune, C. Hotta, J. Takeya, T. Kimura, and Y. Wakabayashi, Nat. Commun. 5:5400 (2014).

[48] K. Momma and F. Izumi, J. Appl. Crystallogr. **44**, 1272 (2011).

Figure caption

Fig. 1. (a) Selected area electron diffraction pattern of MnSi thin film on a Si (111) substrate with the $[111]_{Si}$ incidence. Reflections surrounded by black circles originate only from MnSi thin-film, while those surrounded by yellow circles arise both from MnSi thin film and from Si substrate. The electron diffraction pattern does not have mirror symmetry about the vertical line ($[01\bar{1}]_{Si}$ axis). Positive and negative rotations of the sample around the $[01\bar{1}]_{Si}$ axis are hence not equivalent. (b) Electron diffraction pattern taken with a tilted condition of about 22°. Reflections marked by red and blue circles are attributed to domains with different axis orientations. (c) Schematic drawing of diffraction patterns for the tilted condition at different domains. The observed diffraction pattern corresponds to their superposition. (d) Convergent-beam electron diffraction pattern with $[111]_{Si}$ incidence. Observed intensity distribution is mainly attributable to Si substrate. (e) Simulated convergent-beam electron diffraction pattern of Si. Black and gray arrow heads are for eye-guide to distinguish the crystal orientation.

Fig. 2. Possible configurations of a MnSi thin film on Si (111) substrate and corresponding electron diffraction patterns. Incidence directions are indexed with the MnSi thin film. Upper row shows two possible orientations of crystal axes for [111] and $[\bar{1}\bar{1}\bar{1}]$ incidences, respectively. Simulated electron diffraction patterns with the zone axis incidence and the tilted condition are shown for each configuration. The configurations surrounded by red and blue lines reproduce the result shown in Fig. 1 for domains A (A1 and A2) and B (B1 and B2), respectively.

Fig. 3. Dark-field transmission electron microscope (TEM) image with using (a) reflection

A and (b) reflection B in Fig. 1 (b), respectively. Bright parts in panels (a) and (b) correspond to domains A and B, respectively.

Fig. 4. X-ray reflectivity profile of a thin film of the same batch as the TEM experiment. The simulation using the stacking manner of A2 or B2 (blue line) in Fig. 2 shows better agreement with the experimental result than those of A1 or B1 (red line).

Fig. 5. Schematic drawing of atomic arrangement in A1, A2, B1, and B2. The stacking manner of a thin film of MnSi in A1 and B1 is opposite to that in A2 and B2.

Table 1 Comparison of several methodologies to determine the crystallographic chirality, domain structure, and interface in plane-view of thin-film form with substrate using several techniques.

Plane-view of thin-film form with substrate

	Crystal chirality	Domain structure	Interface
STM [33]		○	△[1]
EBSD [39]	△[2]	○	
CBED [40, 41]	△[3]	△[4]	
SAED + Dark-field TEM image [43]		○	
X-ray reflectance			○
This work: CBED+SAED+ Dark-field TEM image + X-ray reflectance	△[5]	○	○

*1,2,3,4,5

[1] Applicable only if the film is thinner than several nm.
[2] The intensity difference between two enantiomers is mainly observable in the Kikuchi pattern.
[3] Applicable only for the specimen without substrate.
[4] Combination of STEM and CBED can visualize the domain structure.
[5] Applicable only for the sample thinner than about 15 nm.

Fig. 1

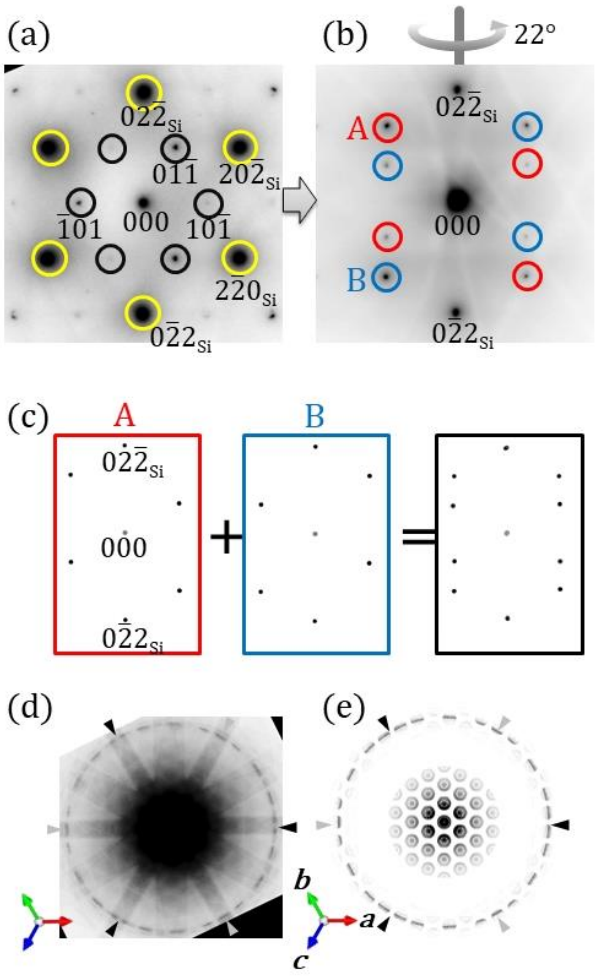
(a)
(b)
22°
$0\bar{2}\bar{2}_{Si}$
$01\bar{1}$
$20\bar{2}_{Si}$
$\bar{1}01$
000
$10\bar{1}$
$2\bar{2}0_{Si}$
$0\bar{2}2_{Si}$
A
B
(c)
A
B
$0\dot{2}\bar{2}_{Si}$
$0\dot{0}0$
$0\dot{2}2_{Si}$
(d)
(e)
b
a
c

Fig. 2

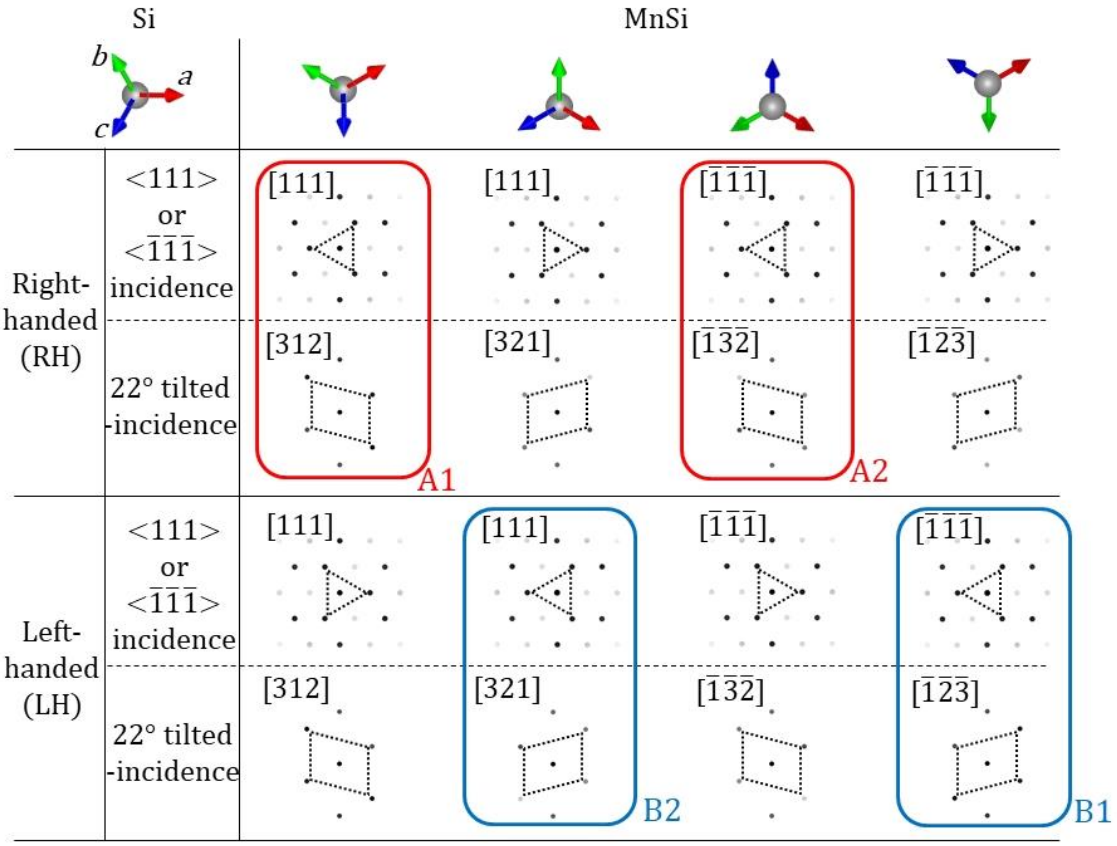
Si
MnSi
b
a
c
Right-handed (RH)
Left-handed (LH)
<111> or <$\bar{1}\bar{1}\bar{1}$> incidence
22° tilted -incidence
[111]
[$\bar{1}\bar{1}\bar{1}$]
[312]
[321]
[$\bar{1}\bar{3}\bar{2}$]
[$\bar{1}\bar{2}\bar{3}$]
A1
A2
B2
B1

Fig. 3

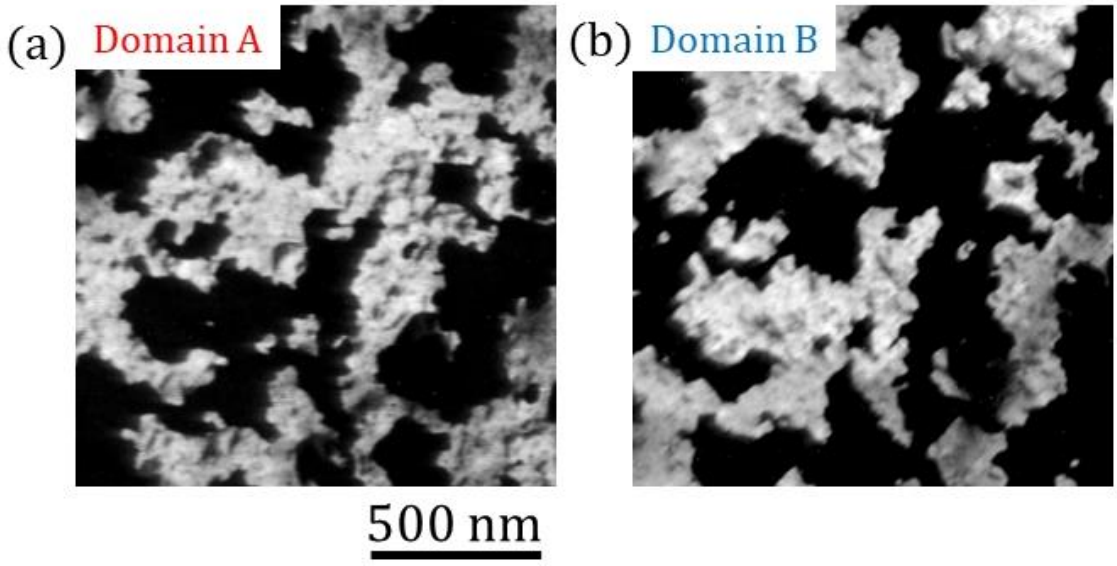

Fig. 4

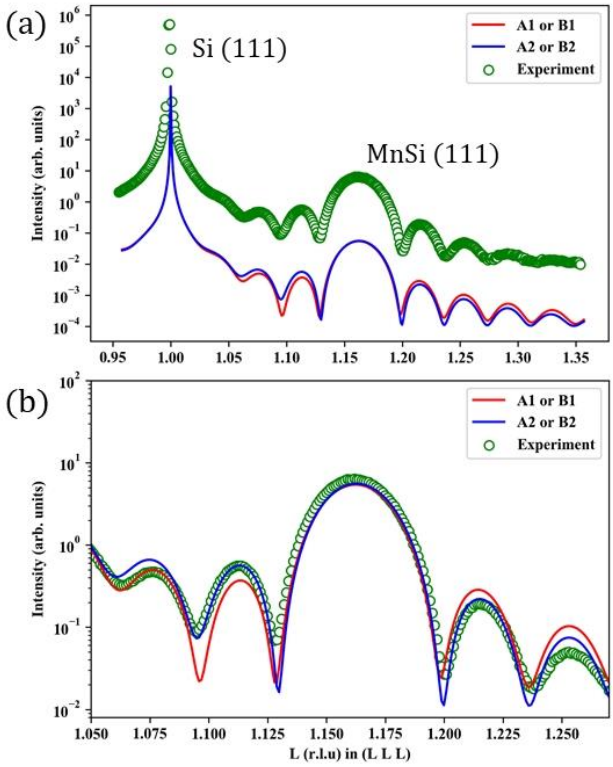
(a)
Si (111)
MnSi (111)
A1 or B1
A2 or B2
Experiment
Intensity (arb. units)
(b)
A1 or B1
A2 or B2
Experiment
Intensity (arb. units)
L (r.l.u) in (L L L)

Fig. 5

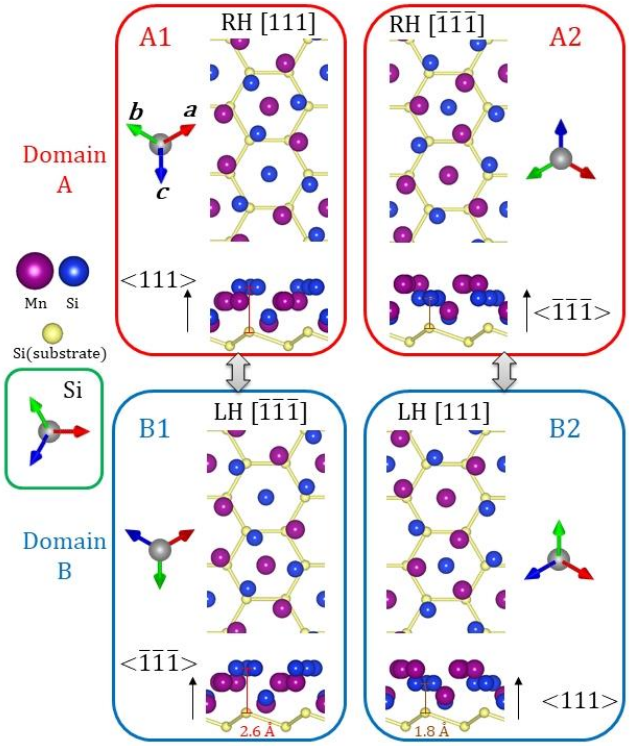
A1
RH [111]
RH [$\bar{1}\bar{1}\bar{1}$]
A2
b
a
c
Domain
A
<111>
<$\bar{1}\bar{1}\bar{1}$>
Mn
Si
Si(substrate)
Si
B1
LH [$\bar{1}\bar{1}\bar{1}$]
LH [111]
B2
Domain
B
<$\bar{1}\bar{1}\bar{1}$>
<111>
2.6 Å
1.8 Å